04;12

Electron energy distribution function in a high-voltage pulsed discharge with an extended hollow cathode

© N.A. Ashurbekov, M.Z. Zakaryaeva, K.O. Iminov, K.M. Rabadanov, G.S. Shakhsinov

Dagestan State University, Makhachkala, Dagestan Republic, Russia
E-mail: nashurb@mail.ru

Received February 28, 2022
Revised March 19, 2022
Accepted March 23, 2022

The dynamics of a nanosecond discharge with an extended hollow cathode in argon is studied and the electron energy distribution function (EEDF) in a plasma column is calculated. The issues of the formation of the EEDF in the discharge column and inside the cathode cavity are considered. The conditions of the validity the two-term approximation of the EEDF in the plasma column are analyzed and the appropriate evaluations are given.

Keywords: hollow cathode, pulse discharge, argon, electron energy distribution function.

DOI: 10.21883/TPL.2022.05.53480.19180

Plasma source based on high-voltage nanosecond discharge with extended hollow cathode at low and medium gas pressures [1,2] can be used in plasma chemistry, in plasma medicine, as well as in various technologies, in particular in technologies of atomic, molecular layer deposition and etching of micro and nano-electronic materials surface (see, for example, [3]).

The main properties and parameters in gas-discharge plasma are mainly determined by the electronic component [4,5]. Therefore, the calculation and analysis of the electron energy distribution function (EEDF) becomes one of the most important issues in the study of unstable unbalanced gas-discharge plasma.

In the present work, a high-voltage pulsed nanosecond discharge is investigated, which is ignited in a discharge chamber, being a quartz tube of diameter 5 cm, where an electrode system of aluminum electrodes, located at a distance of 0.6 cm from each other, is installed. The anode is a flat plate 5 cm long, 2 cm wide and 0.5 cm thick. The cathode is in the form of a cylindrical rod 5 cm long and 1.2 cm in diameter, along which a slit cavity 0.2 cm wide and 0.6 cm deep is cut. The discharge area for the entire length of the electrodes is bounded by dielectric plates of fiberglass [1,2].

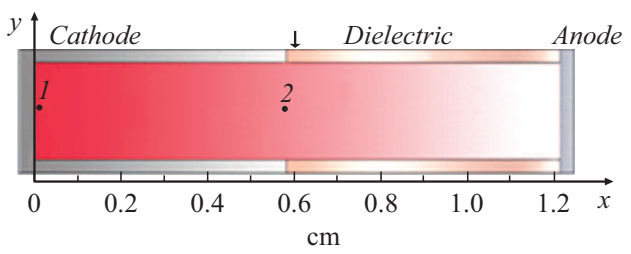

Figure 1. Geometry of the modeling area and location of the points at which the EEDF is calculated.

The geometry of the simulated area corresponded to the real size of the electrode system. The simulation area has a rectangular shape (length 1.2 cm, width 0.2 cm) (Fig. 1).

The EEDF formation mode can be analyzed by introducing a relaxation parameter [6]:

$$K = \left(\nu_e + \delta\nu_{ea} + \nu^*\right)\tau_d, \qquad (1)$$

where τ_d — free diffusion time of electrons to plasma boundaries, ν_e — frequency of electron-electron collisions, ν_{ea} — frequency of elastic electron-atom collisions, ν^* — frequency of inelastic electron-atom collisions, δ — energy exchange factor for elastic collisions. For the conditions considered in this paper (at gas pressure $p = 5$ Torr and applied voltage $U_0 = 1.2$ kV) we obtain the following estimate: $K \approx 50$, $K \gg 1$. This means that in EEDF relaxation, the expansive collision processes prevail over diffusion processes and the mode of EEDF formation is local. The conditions of validity of the two-term EEDF decomposition are [6]:

$$\nu^* \ll \nu_{ea}, \quad eE\lambda/w \ll 1, \quad \lambda \ll L, \qquad (2)$$

where $w = mv^2/2 \sim 6.4 \cdot 10^{-19}$ — kinetic energy of electrons, $\nu_{ea} \sim 3.5 \cdot 10^{10}\,\mathrm{s}^{-1}$ — frequency of elastic collisions of electrons with atoms, $eE\lambda \sim 1.2 \cdot 10^{-19}$ J — energy that an electron gains on a free path. Given that the potential drop of up to 20% of U_0 is in the plasma column, the estimates show that the EEDF formation mode in the plasma column of the simulated discharge is local. In this case, the energy of directional electron motion under the action of the electric field does not exceed the energy of thermal electron motion and the assumption of weak EEDF anisotropy in plasma is valid.

Since even in the case of a strong electric field, the anisotropy of the electron speed distribution remains small, we may restrict ourselves to the classical (local) two-term EEDF approximation, which can be written as follows [7,8]:

$$F(w, \mathbf{r}, t) = \left[f_0(w) + f_1(w)\cos\theta\right] n_e(\mathbf{r}, t), \qquad (3)$$

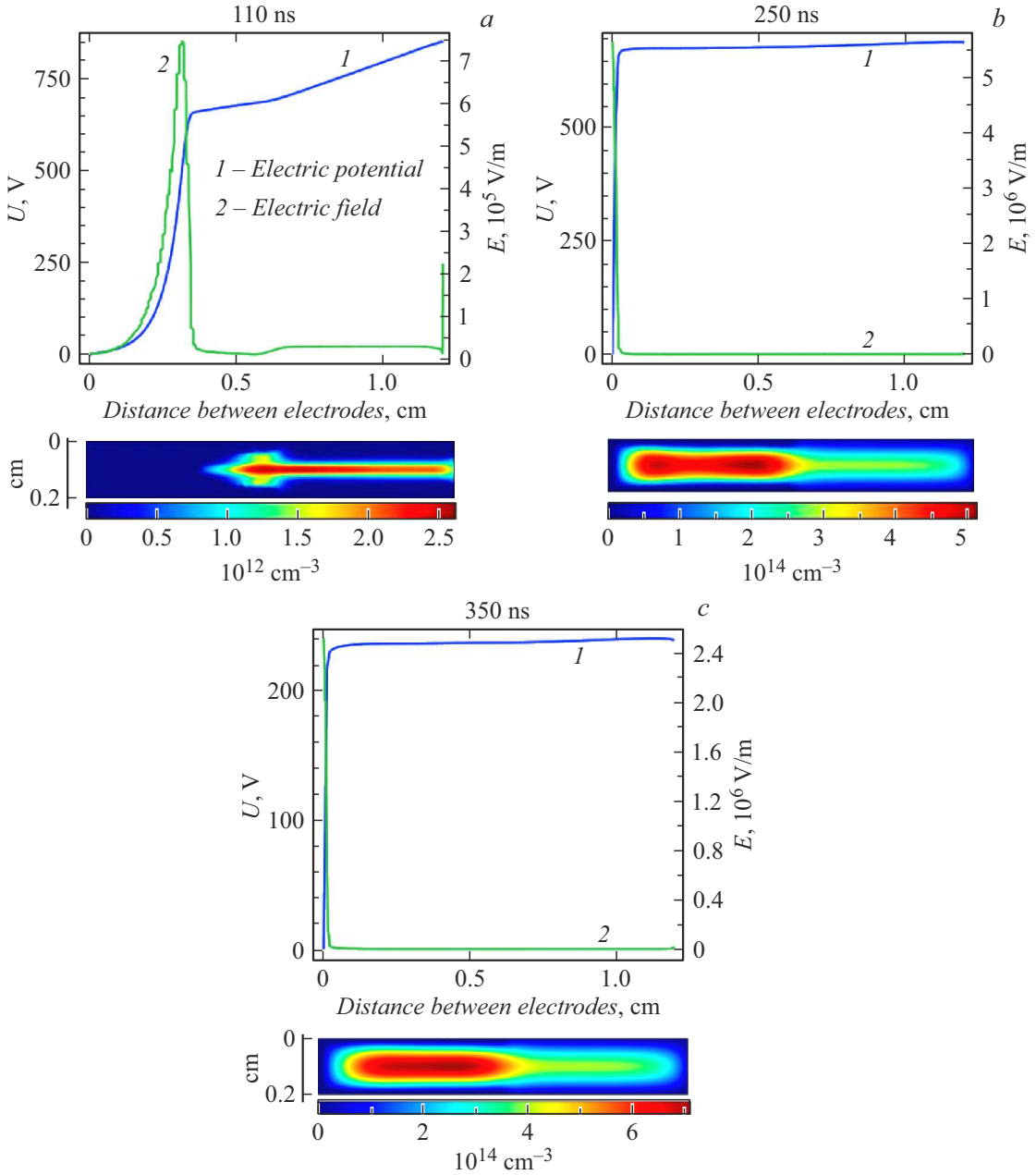

Figure 2. Simulation results of electric field potential, longitudinal electric field and electron density distribution in the discharge gap at different moments of time after the voltage pulse is applied to the discharge gap. *a* — 110 ns, *b* — 250 ns, *c* — 350 ns.

where $f_0(w)$ — is the isotropic part of the electron distribution function, depending only on the change in speed magnitude, $f_1(w)$ — the anisotropic part of the EEDF proportional to the guide cosines of the speed vector, $n_e(\mathbf{r}, t)$ — electron concentrations, $w = m_e v^2/2e$ — kinetic energy (in eV).

For numerical experiments, a computational model has been developed, which includes the Plasma module from COMSOL Multiphysics [8], where the hydrodynamic plasma model was calculated, and the LisbOn KInetics Boltzmann (LoKI-B) [9], where the Boltzmann kinetic equation was solved and the EEDF was calculated. The LoKI-B program has been adapted to calculate the EDEF in our problem. The LoKI-B program from the COMSOL program module obtained values of the reduced electric field, gas pressure and temperature, electron and ion densities, distributions of excited state populations of the working gas, and corresponding sets of electron scattering cross sections as input parameters at each time and point in the problem solution region, which were used to solve the kinetic equation. A detailed algorithm for the numerical solution of the Boltzmann equation is presented in [9,10]. The Boltzmann equation is discretized, and its solution is found using a finite-difference scheme.

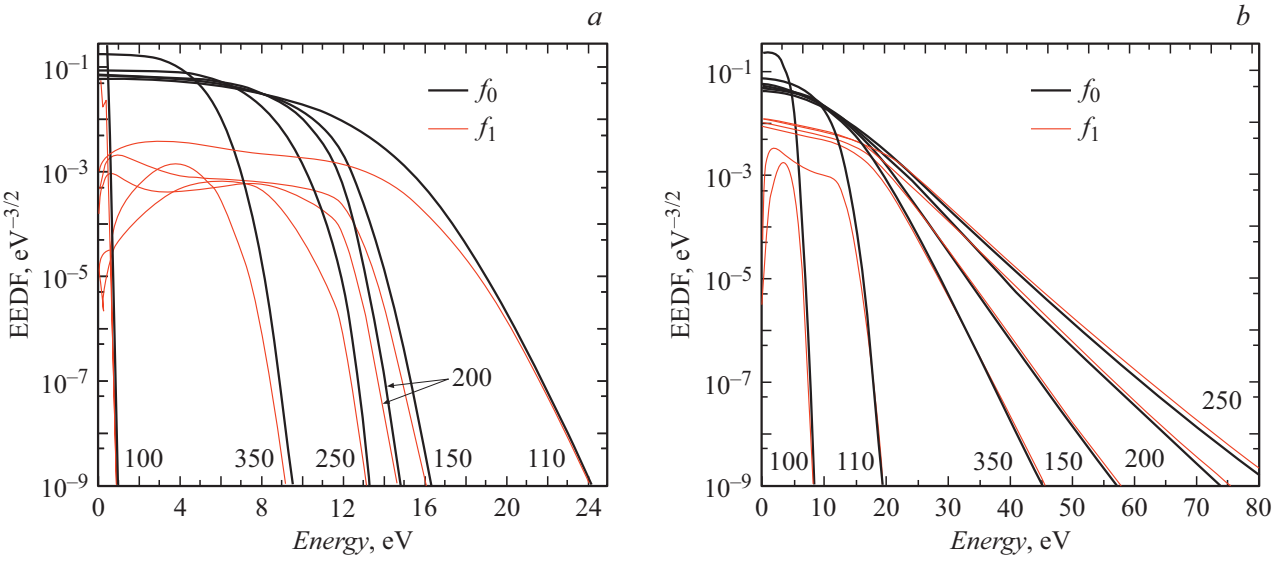

Figure 3. Isotropic $f_0(w)$ and anisotropic $f_1(w)$ parts of the EEDF at points 0.6 (a) and 0.1 cm (b) from the cathode slit base at different points in time (given in ns near the curves).

Figure 2 shows the results of modeling the distribution of the electric field potential, the longitudinal electric field, and the electron density in the gap and in the cathode cavity.

The results of the simulation of the dynamics of the space-time electron density distribution show that about 80 ns after applying voltage to the gap at the anode surface, a plasma clot forms in the center with a $\sim 10^9\,\mathrm{cm}^{-3}$. Then, the ionization wave starts from this point and propagates toward the cathode. As the ionization wave propagates, the electron density at the front and behind the front of the ionization wave increases. The propagation speed of the ionization front is on the order of $\sim 2 \cdot 10^7$ cm/s, and after about 100 ns, it reaches the cathode surface [11]. By the time of 110 ns the electron concentration reaches $\sim 10^{12}\,\mathrm{cm}^{-3}$ and the ionization wave front penetrates into the cathode cavity (Fig. 2, a), then the ionization wave spreads along the cavity side surfaces and reaches the cavity bottom. Then, a reverse ionization wave is formed from the cavity bottom, which leads to the formation of a plasma column in the cathode cavity and in the discharge gap. Figure 3 shows the results of EEDF calculations obtained at two points in the center of the gas-discharge system at different distances from the bottom of the hollow cathode: point *1* is located inside the hollow cathode at 0.1 cm from its bottom; point *2* is located at 0.6 cm from the bottom of the hollow cathode at the cathode-dielectric interface (Fig. 1).

Figure 3, a shows the EEDF calculated at point *2*. The figure shows that at time 100 ns the EEDF has not yet been formed because the ionization wave has not yet reached this point. Already after 10 ns by the time of 110 ns the EEDF is formed, and this time coincides with the arrival time of the ionization wave at the point *2* (Fig. 2, a). It can be seen that both the isotropic and the anisotropic parts of the EEDF have strongly increased, and the tail of the anisotropic part of the EEDF is compared with the tail of the isotropic part. This means that at a given time, accelerated electrons start forming in this point. When an ionization wave propagates, almost the whole electric field is concentrated at the surface of this wave. Free electrons are accelerated, gain energy in this region of the reinforced electric field and lead to EEDF deformation with an increase in the high-energy part. Further, over time, it can be seen that both isotropic and anisotropic EEDF start to decline. This means that the ionization wave has passed and the number of fast electrons begins to decrease (Fig. 3, a).

Figure 3, a shows the EEDF calculated at point *1* (Fig. 1). The figure shows that at time 100 ns, the EEDF has not yet been formed because the ionization wave has not yet reached this point and there are very few fast electrons. Further, you can see that over time the EEDF becomes hollow. At the moment of time 150 ns, the tail of the anisotropic part of the EEDF starts to exceed the tail of the isotropic part of the EEDF. This means that at a given time, high-energy electrons arrive at that point along with the ionization wave. Then, the high-energy part of the EEDF continues to grow, and by the time of 250 ns it reaches its maximum. The EEDF becomes strongly gentle, the tail of the anisotropic part of the EEDF is noticeably larger than the isotropic part (Fig. 3, b). This indicates that a beam of fast electrons additionally arrives at the point *1* at time 250 ns and enriches the EEDF. It is known that one of the distinctive features of the hollow-cathode discharge is a sharp decrease of the cathode potential fall (CPF) region as compared to the case of an ordinary anomalous glow discharge. Its dimensions are such that the electrons emitted by the cathode pass through the CPF region almost without collisions and acquire energy $\varepsilon = eU_k$, where U_k — potential of the cathode layer [1,11,12]. Let us estimate

the CPF region size for the discharge conditions under study. Using the ratio $d_k p \approx 7.5 \cdot 10^{-2}\,\text{cm} \cdot \text{Torr}$ [12], we get $d_k \approx 1.5 \cdot 10^{-2}\,\text{cm}$ — length of the CPF region. The value of d_k is comparable to the value of the free path length of electrons with respect to inelastic processes $\lambda^* = 1/(N\sigma^*) \approx 3 \cdot 10^{-2}\,\text{cm}$, where $N = 3.3 \cdot 10^{16} p\,[\text{Torr}]\,\text{cm}^{-3}$, $\sigma^* \approx 2 \cdot 10^{-16}\,\text{cm}^2$. Consequently, the electrons emitted by the cathode pass through the CPF region without collisions and acquire energy $\varepsilon \sim 650\,\text{eV}$ (Fig. 2, *b*). Indeed, as noted above, by this time, the cathode layer is completely formed in the cathode cavity, and the electrons accelerated in the CPF region also form EEDF at the point *1*.

Thus, calculations show that in the gap between the electrodes and at the entrance to the cathode cavity, the EEDF is formed by plasma electrons and electrons accelerated at the ionization wave front. In the cathode cavity, electrons accelerated in the CPF region make a significant contribution to the formation of EEDF, which enrich the high-energy part of EEDF. The calculation results confirm the formation of high-energy electrons in this type of discharges and show the effectiveness of this technique for calculating the EEDF in the plasma column of similar types of gas discharges, but the EEDF calculations in the cathode layer of the discharge require additional research [13,14].

Funding

This work was financially supported by grant of the Russian Foundation for Basic Research № 19-32-90179 and by State Task FZNZ-2020-0002.

Conflict of interest

The authors declare that they have no conflict of interest.

References

[1] N.A. Ashurbekov, K.O. Iminov, O.V. Kobzev, V.S. Kobzeva, Tech. Phys., **55** (8), 1138 (2010). DOI: 10.1134/S1063784210080104.
[2] N.A. Ashurbekov, K.O. Iminov, in *Generation of runaway electron beams and X-rays in high pressure gases*, ed. by V.F. Tarasenko (Nova Publ., N.Y., 2016), vol. 1, p. 421.
[3] A. Agarwal, K. Bera, J. Kenney, A. Likhanskii, S. Rauf, J. Phys. D: Appl. Phys., **50** (42), 424001 (2017). DOI: 10.1088/1361-6463/aa88f0
[4] V.I. Kolobov, L.D. Tsendin, Phys. Rev. A., **46** (12), 7837 (1992). DOI: 10.1103/PhysRevA.46.7837
[5] Y.B. Golubovskii, I.A. Porokhova, J. Benke, J.P Benke, J. Phys. D: Appl. Phys., **32** (4), 456 (1999). DOI: 10.1088/0022-3727/32/4/016
[6] L.D. Tsendin, UFN, **180** (2), 139 (2010). DOI: 10.3367/UFNr.0180.201002b.0139 [L.D. Tsendin, Phys. Usp., **53** (2), 133 (2010). DOI: 10.3367/UFNe.0180.201002b.0139].
[7] M.A. Lieberman, A.J. Lichtenberg, *Principles of plasma discharges and materials processing* (Wiley, N.Y., 2005).
[8] *COMSOL Multiphysics Reference Manual, version 5.5*, COMSOL, Inc. www.comsol.com
[9] A. Tejero-del-Caz, V. Guerra, D. Goncalves, M. Lino da Silva, L. Marques, N. Pinhão, C.D. Pintassilgo, L.L. Alves, Plasma Sources Sci. Technol., **28** (4), 043001 (2019). DOI: 10.1088/1361-6595/AB0537
[10] https://github.com/IST-Lisbon/LoKI
[11] N.A. Ashurbekov, K.O. Iminov, G.Sh. Shakhsinov, M.Z. Zakaryaeva, K.M. Rabadanov, Plasma Sci. Technol., **22** (12), 125403 (2020). DOI: 10.1088/2058-6272/abbb78
[12] N.A. Ashurbekov, K.O. Iminov, O.V. Kobzev, V.S. Kobzeva, Tech. Phys. Lett., **33** (6), 517 (2007). DOI: 10.1134/S1063785007060211
[13] A.S Mustafaev, Tech. Phys., **46** (4), 472 (2001). DOI: 10.1134/1.1365475
[14] R. Winkler, G.L. Braglia, A. Hess, J. Wilhelm, Beitr. Plasmaphys., **25** (4), 351 (1985). DOI: 10.1002/ctpp.19850250405